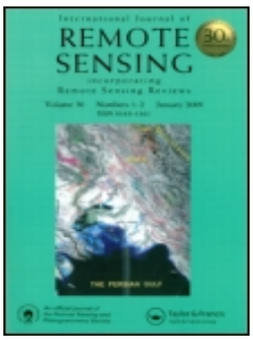

International Journal of Remote Sensing

ISSN: 0143-1161 (Print) 1366-5901 (Online) Journal homepage: http://www.tandfonline.com/loi/tres20

Analysis of spatial distribution pattern of change-detection error caused by misregistration

Wenzhong Shi & Ming Hao

To cite this article: Wenzhong Shi & Ming Hao (2013) Analysis of spatial distribution pattern of change-detection error caused by misregistration, International Journal of Remote Sensing, 34:19, 6883-6897, DOI: 10.1080/01431161.2013.810353

To link to this article: http://dx.doi.org/10.1080/01431161.2013.810353

International Journal of Remote Sensing, 2013
Vol. 34, No. 19, 6883–6897, http://dx.doi.org/10.1080/01431161.2013.810353

Analysis of spatial distribution pattern of change-detection error caused by misregistration

Wenzhong Shi[a] and Ming Hao[b]*

[a]*Joint Research Laboratory on Spatial Information, The Hong Kong Polytechnic University and Wuhan University, Wuhan and Hong Kong, China;* [b]*School of Environment Science and Spatial Informatics, China University of Mining and Technology, Xuzhou, China*

(*Received 14 December 2012; accepted 7 May 2013*)

Misregistration between multitemporal remotely sensed images is one of the significant sources of change-detection errors. In this study, spatial distribution of change-detection errors induced by misregistration was analysed quantitatively. First, multitemporal images are registered with different misregistration values measured by root mean square error (RMSE) from 0 to 1 pixels. The image differencing method, one of the most widely used change-detection methods, is then used to detect changes. Finally, the spatial distribution pattern of change-detection errors caused by misregistration is analysed using buffering analysis based on multitemporal image edges. Experimental results indicate that the commission errors caused by misregistration values from 0 to 1 pixels are almost always within 1 pixel of the edge, regardless of image resolution. In addition, the omission errors falling within 1 pixel of the edges are about 70% for medium-resolution images. The omission errors falling within 1 or 2 pixels of the edges for high-resolution images can be as much as 50% to 60%. This work improves the understanding of spatial distribution of change-detection errors caused by misregistration and shows the relations between these errors and image edges. Moreover, it is helpful for developing new methods by combining edge and spatial information to reduce the adverse effects of misregistration on change-detection.

1. Introduction

With the development of spatial technology, remote sensing is now used more widely, and change detection is one of the most important applications. Change detection identifies change by comparing the reflectance or intensity values of two or more remotely sensed images taken at different times of the same geographical area. Moreover, it is widely used to detect disasters, monitor environmental changes, and identify land use/land cover changes. Of the many different change-detection methods, the most widely used involve image differencing, change vector analysis (CVA), image rationing, image regression, and principal component analysis (PCA) (Singh 1989; Lu et al. 2004).

For the majority of change-detection methods, the registration of multitemporal images is a necessary process, which is a procedure for aligning multitemporal images. More importantly, registration accuracy markedly affects change-detection accuracy. Reducing the effects of misregistration and subsequent improvement in change-detection accuracy has attracted much interest. It is clear that high levels of registration must be achieved

*Corresponding author. Email: haomingcumt@gmail.com

if there is to be reliable global change monitoring (Townshend et al. 1992). According to Dai and Khorram (1998), change-detection errors of less than 10% can be obtained if there is a registration accuracy of less than one-fifth of a pixel. To reduce the effects of misregistration, a model that compensates for misregistration effects on change-detection results has been proposed and used to improve change-detection accuracy (Stow 1999; Stow and Chen 2002). Sundaresan et al. have found that the change-detection algorithm based on Markov random field (MRF) is more robust to registration noise than the image-differencing method (Sundaresan, Varshney, and Arora 2007). Brown et al. reduced the impact of geometric errors and misregistration by modelling geometric and misregistration errors in airborne sensor data (Brown, Foody, and Atkinson 2007). Various novel registration methods have been proposed to reduce registration noise (Bruzzone and Cossu 2003; Stow, Coulter, and Baer 2003; Ding et al. 2010; Marchesi, Bovolo, and Bruzzone 2010).

Many studies also have made contributions to reduction of the impact of imprecise registration on change detection. Their conclusions, however, reveal only the relationship between change-detection accuracy and registration errors. Dai and Khorram (1998) indicated that false changes resulting from misregistration are distributed spatially mainly along the edges of remotely sensed images, but missed changes resulting from misregistration are spatially distributed distant from edges. However, the spatial distribution of change-detection errors resulting from misregistrations has not yet been studied in detail and quantifiably. This study focussed on the spatial distribution of change-detection errors at different misregistration values measured by root mean square error (RMSE) using the buffering analysis technique. In the first phase, the image differencing method is implemented to generate difference images using multitemporal images with different misregistrations. The best change-detection results are produced based on thresholds determined manually. At the same time, change-detection errors are easily obtained based on reference data. In the second phase, buffer zones are created based on multitemporal image edges derived by the Canny algorithm (Canny 1986), and the percentages of change-detection errors falling within the buffer zones are calculated. Finally, it is anticipated that the objective of understanding the spatial distribution laws of change-detection errors due to misregistration will be achieved.

The article is organized as follows. The second section introduces the study methodology including simulating the different misregistration, change-detection methods, and buffering analysis. In Section 3, the data sets used in the experiments are presented in detail and the experimental results are also reported. Section 4 presents a discussion of the experimental results, and conclusions are drawn in Section 5.

2. Methodology

2.1. Simulating misregistration

Image registration is a procedure for aligning multitemporal images. The registration process is usually performed using a polynomial algorithm by ground control points (GCPs), where the relationship between the original and registered images is given thus:

$$\begin{cases} x = a_0 + a_1 X + a_2 Y \\ y = b_0 + b_1 X + b_2 Y \end{cases}, \tag{1}$$

where (x,y) and (X,Y) are the corresponding pixels of the original and registered images, and a_0, a_1, a_2, b_0, b_1, and b_2 are constants. The differences between two images

including scale, rotation, translation, and small nonlinear transformations are described in Equation (1). In this study, both rotation and translation are considered because registration errors may become manifest on account of image translations and rotations (Sundaresan, Varshney, and Arora 2007). Both translation and rotation misregistration can be simulated by sliding the registered image relative to the original image in both the x and y directions. As it is known that most widely used registration algorithms can achieve registration at sub-pixel accuracy, misregistration values from 0 to 1 pixels in steps of 0.2 pixels were introduced in this study.

The registered image is shifted in both x and y directions by steps of 0.2 to simulate misregistration (Dai and Khorram 1998; Sundaresan, Varshney, and Arora 2007). The sliding values in the x and y directions are generated randomly each time, but the total degree of misregistration should conform to the particular misregistration value. The registered image is then resampled. The resampling is a necessary process for sub-pixel registration and its effect should be considered. In this work, bilinear interpolation, a commonly used approach for resampling (Zitova and Flusser 2003), is adopted. In the registration process of other studies, this resampling method can also be used and the outcomes of this study are applicable to this condition.

2.2. Change-detection method

In this study, the image-differencing method, one of the most widely used change-detection techniques, was adopted. This method detects changes based on difference in image generated by subtracting one image from another, both acquired in the same geographic area at different times. If $f_1(x,y)$ and $f_2(x,y)$ are the two images at different times, the difference image $f_D(x,y)$ is given by

$$f_{\mathrm{D}}(x,y) = |f_1(x,y) - f_2(x,y)|. \tag{2}$$

Further analysis is made to the difference image to find changes by determining a threshold. The determination of threshold values remains an active research topic, and more and more automatic methods are being introduced to solve the problem (Bruzzone and Prieto 2000; Melgani and Bazi 2006; Bazi, Melgani, and Al-Sharari 2010). This is not the central topic of this research, however, and so the traditional manual approach to threshold determination (Bruzzone and Serpico 1997; Bruzzone and Cossu 2003) was therefore taken:

$$f_{\mathrm{D}}(x,y) - m \geq T_{\mathrm{d}} \cdot \sigma, \tag{3}$$

where m is the mean grey value of the difference image, σ represents the standard deviation of the difference image, and T_{d} is a constant to determine the threshold. If the difference image grey value conforms to the condition above, those pixels are identified as changes. Based on Equation (3), a manual trial-and-error procedure is utilized to find the optimal threshold. The value of T_{d} ranges from –3 to 3 in steps of 0.25 and the threshold, resulting in the minimum overall error compared to the reference map, is selected as the optimal threshold.

Change-detection errors induced by misregistration may be either false changes caused or true changes removed. Four indices were used to evaluate the accuracy of change-detection results.

(1) The percentage of correct change detection (PCCD) is defined as the ratio of the total number of pixels correctly detected as being changed to the total number of pixels detected as being changed.
(2) The percentage of missed alarms (PMA) is defined as the ratio of the number of changed pixels wrongly detected as unchanged (omission errors) to the total number of pixels that have changed in the ground-truth data.
(3) The percentage of false alarms (PFA) is defined as the ratio of the number of unchanged pixels that are wrongly detected as changed (commission error) to the total number of pixels that have not changed in the ground-truth data.
(4) The percentage of total error (PTE) is defined as the ratio of the total number of wrongly detected pixels to the total number of pixels in the image.

2.3. Buffering analysis

In this study, the focus was on the spatial distribution of commission and omission errors. Since Dai and Khorram found that commission errors occur along the image edges and omission errors occur away from the image edges, the distribution of change-detection errors was analysed quantitatively for different misregistration values using buffering analysis based on image edges. First, the Canny algorithm is used to detect the edges of multitemporal images. The edges of multitemporal images are combined together as the last edges to build the buffer. Second, a buffer zone is created based on the last edges with a buffer distance. Third, the percentages of commission, omission, and total errors falling within the buffer zone are computed as measures of the spatial distribution of change-detection errors caused by misregistration, recorded as PCEB, POEB, and PTEB, respectively.

3. Experimental results

3.1. Experimental data sets

3.1.1. Data set 1

The first of three data sets used in the experiments were images acquired by Landsat Thematic Mapper (TM) in the west of Lesser Khingan, China. The t_1 image (650 × 700 pixels) was acquired in August 2006, and the t_2 image was artificially generated based on the t_1 image by introducing changes. Figures 1(*a*) and (*b*) show band 4 of the t_1 and t_2 images, respectively, and the true ground changes are shown in Figure 1(*c*) as a reference image.

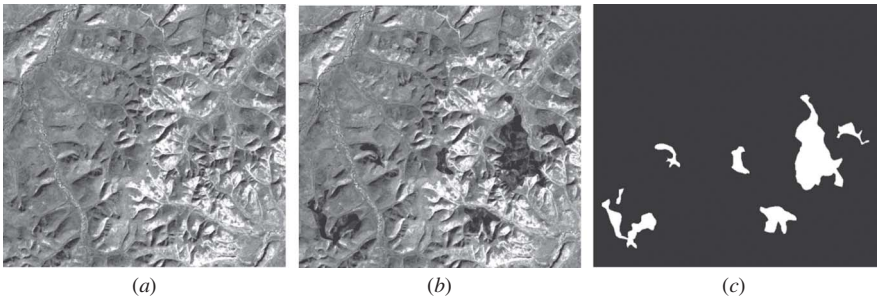

(*a*) (*b*) (*c*)

Figure 1. Synthetic data set 1: (*a*) t_1 image acquired by Landsat TM sensor in August 2006, (*b*) synthetic t_2 image, and (*c*) true ground data.

3.1.2. Data set 2

The second data set was acquired by the Landsat Enhanced Thematic Mapper Plus (ETM+) sensor in August 2001 in the middle of Liaoning Province, China, as the t_1 image (400 × 400 pixels). The t_2 image was generated by introducing changes artificially. Band 4 of t_1 and t_2 images is shown in Figures 2(*a*) and (*b*), respectively, and Figure 2(*c*) shows the ground-truth changes.

3.1.3. Data set 3

The image acquired by Quickbird in 2005 was used in the study as the third data set in the south of Xuzhou, China, as the t_1 image (1000 × 1000 pixels) and the t_2 image was also generated by introducing changes artificially. The panchromatic bands of t_1 and t_2 images are shown in Figures 3(*a*) and (*b*). The ground-truth changes are displayed in Figure 3(*c*).

3.2. Experimental results

3.2.1. Data set 1

Misregistrations in the *x* and *y* directions were generated randomly, to satisfy the particular RMSE from 0 to 1 pixels in steps of 0.2 pixels, for the t_1 image and t_2 image registrations. After that, the image difference method was applied to the registered images, and a manual trial-and-error process was adopted to yield the best change-detection results. Figures 4(*a*) and (*b*) show the change-detection accuracy patterns for PCCD, PFA, PMA, and PTB.

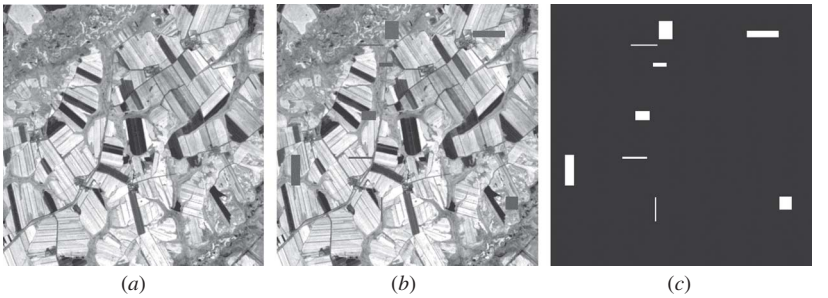

(*a*) (*b*) (*c*)

Figure 2. Data set 2: (*a*) t_1 image acquired by Landsat ETM+ sensor in August 2001, (*b*) synthetic t_2 image, and (*c*) ground-truth data.

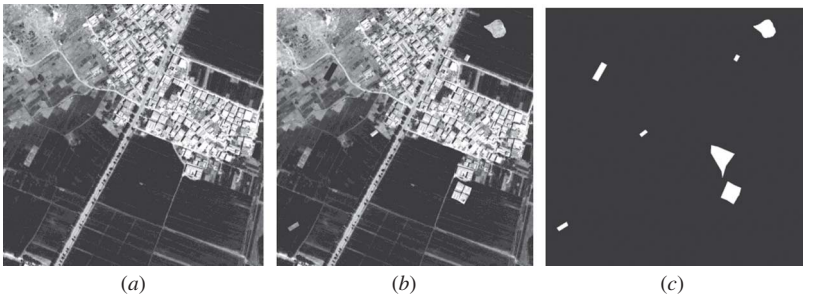

(*a*) (*b*) (*c*)

Figure 3. Synthetic data set 3: (*a*) t_1 image acquired by Quickbird in 2005, (*b*) synthetic t_2 image, and (*c*) ground-truth data.

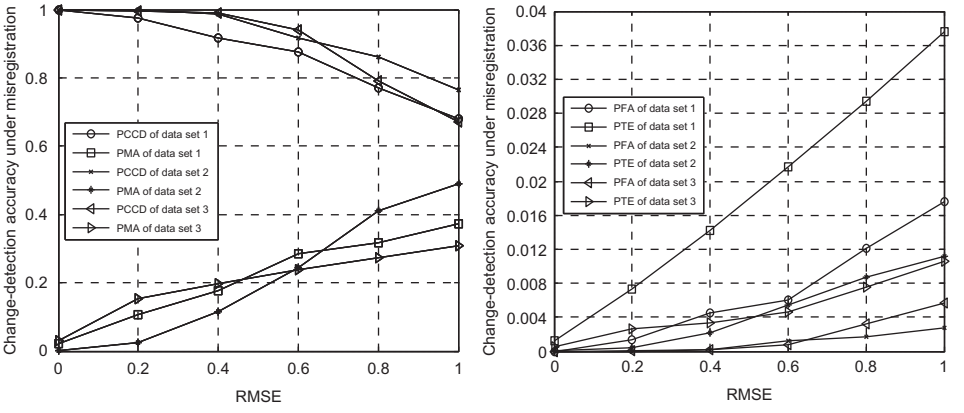

Figure 4. Accuracy of change-detection results for different misregistration values for the three data sets: (*a*) change patterns of PCCD and PMA and (*b*) change patterns of PFA and PTE.

As can be seen, PCCD drops with increasing misregistration values, reaching 0.9 when the value of RMSE is 0.4. On the contrary, PMA increases with increasing misregistration values. PFA and PTE look small only by contrast, because the changes are small and the image is large and they also increase with increasing misregistration. The situation conforms to all the other research conclusions.

To analyse the spatial distribution of change-detection errors as described above, the image edges were detected using the Canny algorithm and the buffer zone was created based on the last edges with buffer distance values of 1, 2, and 3 pixels, respectively. The last edges were generated by combining edges of t_1 and t_2 images. In this condition, the change-detection errors corresponding to MRSE from 0 to 1 pixels are shown together with the buffer zone in Figure 5. The calculated commission, omission, and total error percentages falling within the buffer zone are also displayed for each RMSE, with different buffer distance values, in Figure 6.

As can be seen from Figure 4, when the images were registered without misregistration, the change-detection accuracy was very high. At this point, few omission errors and no commission errors occurred, as shown in Figure 5(*a*). Since there were no commission errors, PCEB was empty and POEB and PTEB had the same value of 70%, as shown in Figure 6(*a*). For other misregistration values, PCEB was close to 100%, which meant that almost all commission errors caused by misregistration fell within the buffer zone, and the values of POEB and PTEB remained close to 70% and 80%, respectively, as shown in Figures 5 and 6(*a*). The detailed spatial distribution of commission and omission errors with 0.8 MRSE is shown in Figures 5(*g*) and (*h*), by enlarging two areas of Figure 5(*e*).

When the buffer distance value was 2, almost all commission errors also fell within the buffer zone, and both POEB and PTEB started at 95% without misregistration and dropped with increasing MRSE, finally reaching 90% and 95%, respectively, as shown in Figure 6(*b*). For distance value 3, all change patterns of PCEB, POEB, and PTEB were similar to those with a buffer distance value of 2, but they become larger for the same MRSE value, as shown in Figure 6(*c*).

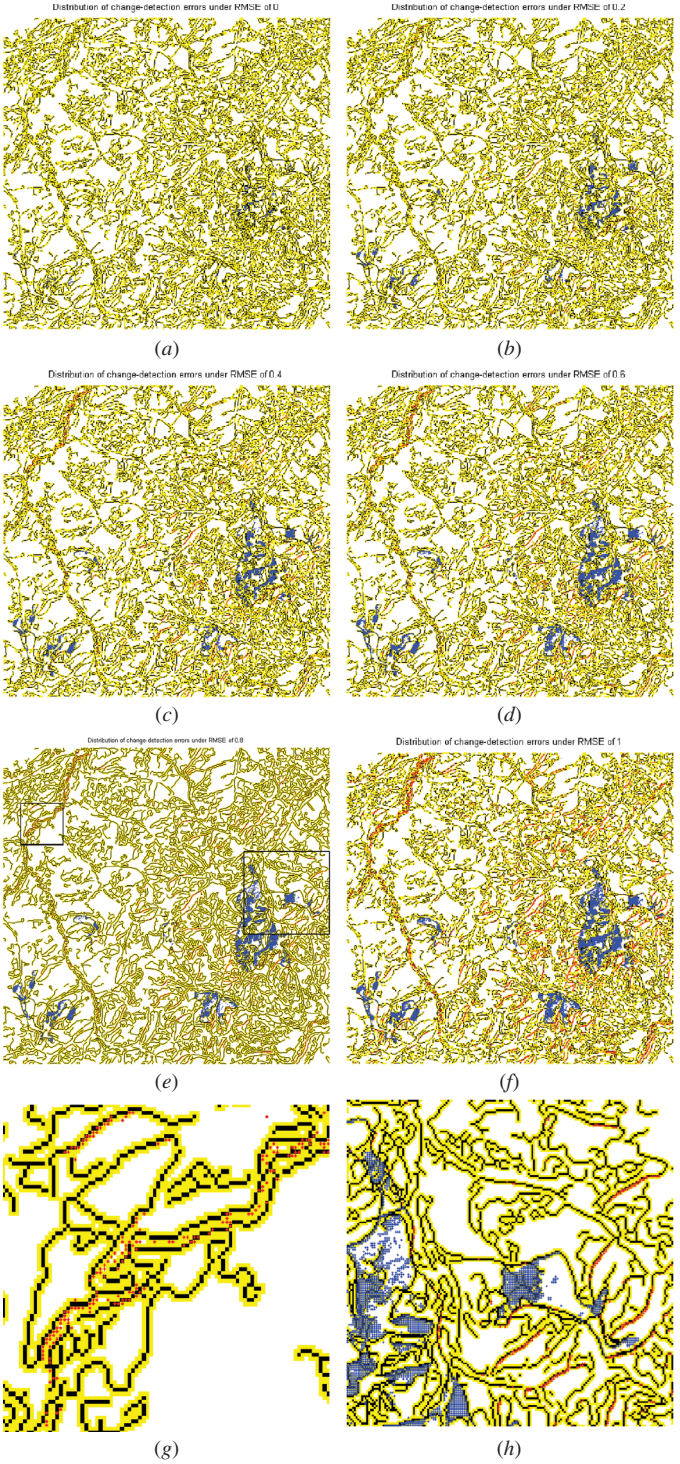

Figure 5. Spatial distribution of change-detection errors caused by misregistration based on buffer zone for RMSE values from 0 to 1 pixels in steps of 0.2 pixels corresponding to cases (*a*) to (*e*); (*g*) and (*h*) are enlarged views of the left and right boxes in (*e*).

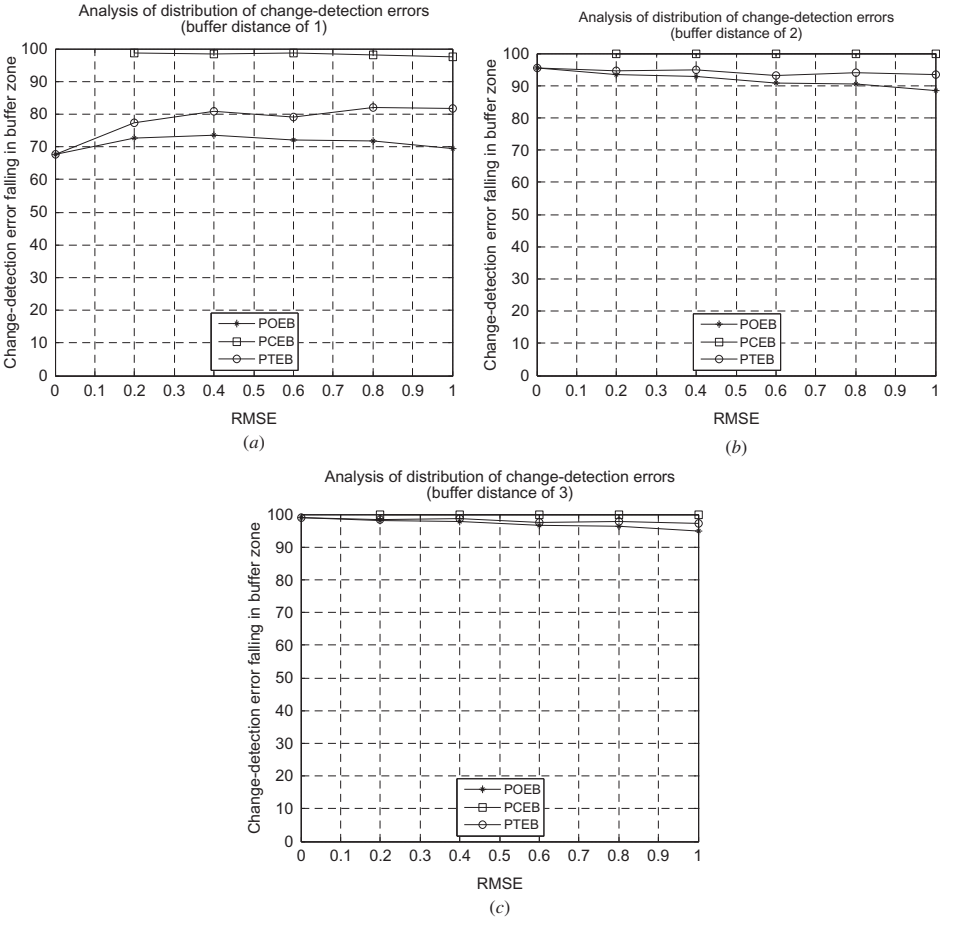

Figure 6. Percentage of change-detection errors including commission, omission, and total errors for different misregistrations falling within the buffer zone, with different buffer distance values from 1 to 3 corresponding to (*a*) to (*c*).

3.2.2. Data set 2

As indicated above, misregistrations were simulated from 0 to 1 pixels when the images acquired by the Landsat ETM+ sensor were registered. Given that, the image difference method was also applied to the registered images, and a manual trial-and-error procedure was used to generate best change-detection results. Figures 4(*a*) and (*b*) show the change-detection accuracy patterns for PCCD, PMA, PFA, and PTB for different misregistration values. It can be seen that PCCD also decreased with increasing misregistration. Moreover, PMA, PFA, and PTE increased with increasing misregistration.

The image edges were detected using the Canny algorithm, and buffer zones were created at buffer distance values of 1, 2, and 3 pixels based on combined edges. The buffer zone with one pixel distance was also taken as a detailed example to assess the spatial distribution of change-detection errors caused by misregistration. The change-detection errors for different RMSE values are shown in Figure 7, together with buffer zones, and the percentages of commission, omission, and total errors falling within the buffer zone for different RMSE values are shown for buffer distance value 1, as shown in Figure 8(*a*).

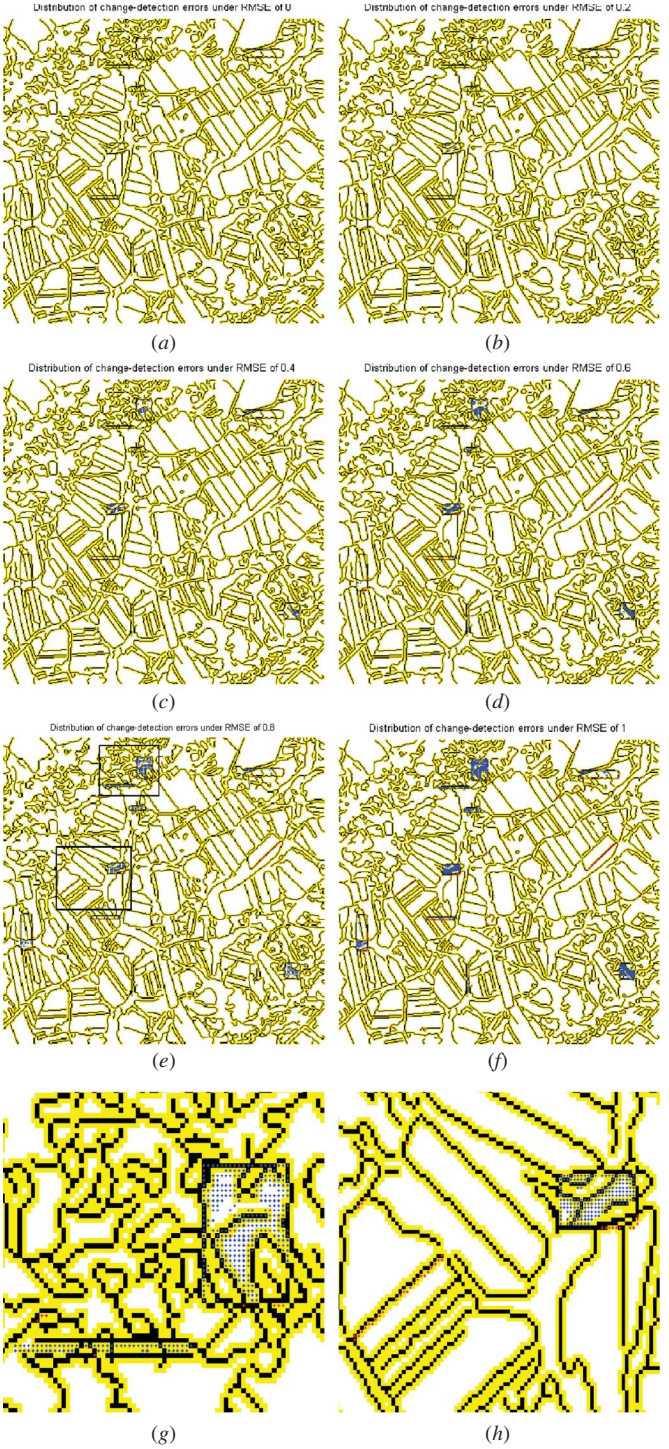

Figure 7. Spatial distribution of change-detection errors caused by misregistration based on buffer zone for RMSE values from 0 to 1 pixels in steps of 0.2 pixels, corresponding to (*a*) to (*e*); (*g*) and (*h*) are enlarged views of upper and lower boxes in (*e*).

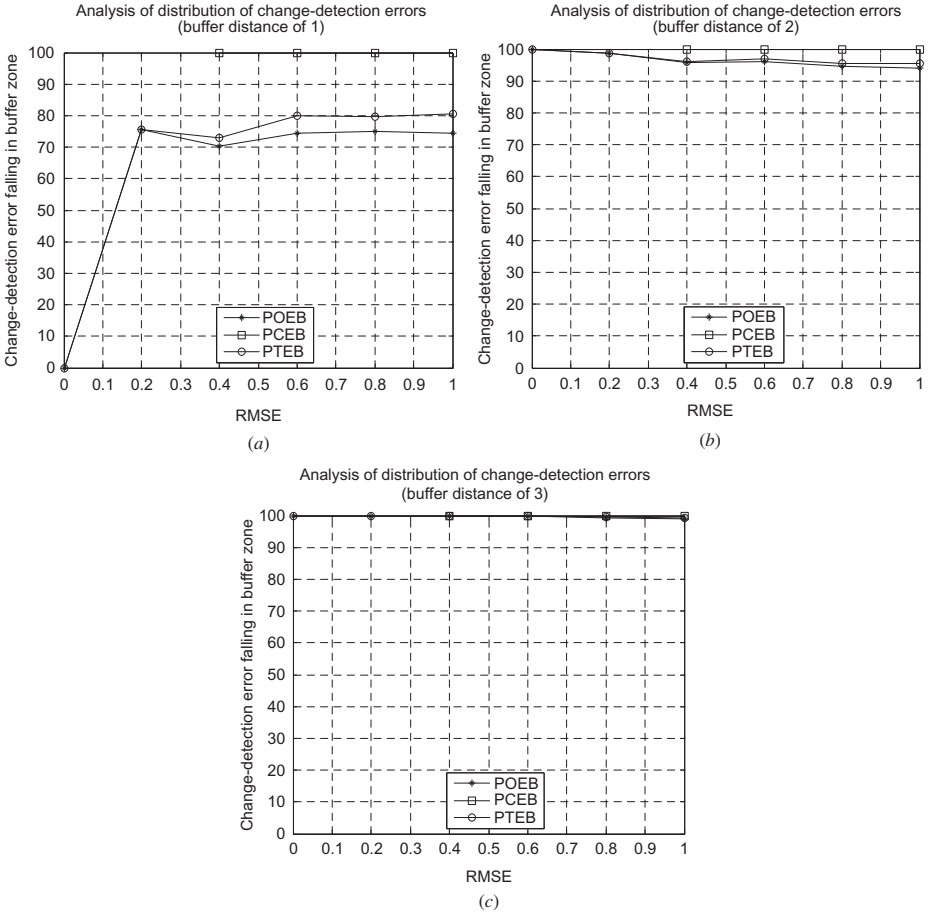

Figure 8. Percentage of change-detection errors including commission, omission, and total errors for different misregistrations falling within the buffer zone, with different distance values from 1 to 3 corresponding to (*a*) to (*c*).

As can be seen, when the images were registered with no applied misregistration, there were virtually no errors, as shown in Figures 4 and 7(*a*). Consequently, PCEB was empty and POEB and PTEB were 0 at this point, as shown in Figure 8(*a*). When the value of RMSE reached 0.6, the commission errors caused by misregistration almost all fell within the buffer zone, and POEB and PTEB were close to 75% and 80%, respectively, as shown in Figures 7(*d*) and 8(a). When the value of RMSE was 1, nearly all commission errors still fell within the buffer zone, and PTEB and PTEB remained close to 75% and 80%, respectively, as shown in Figures 7(*f*) and 8(*a*). In short, for different misregistrations, almost all commission errors caused by misregistration fall within the buffer zone, and the values of PTEB and PTEB were nearly always close to 75% and 80%, respectively. Two areas of the spatial distribution of errors are enlarged with 0.8 RMSE, as shown as Figures 7(*g*) and (*h*).

When the buffer distance value was 2, almost all commission errors fell within the buffer zone, and both PTEB and PTEB started at 100% in the case of no misregistration and decreased with increasing degree of misregistration down to a final level of 95%, as

shown in Figure 8(*b*). For distance value 3, we can see from Figure 8(*c*) that PCEB, PTEB, and PTEB were close to 100%, meaning that both commission and omission errors almost fell within the buffer zone.

3.2.3. Data set 3

Data set 3 was Quickbird images, and simulated misregistrations were introduced between the t_1 and t_2 images from 0 to 1 pixels in steps of 0.2 pixels. As above, the image-difference method was then applied to the registered images and a manual trial-and-error procedure was performed to obtain optimal change-detection results. Figures 4(*a*) and (*b*) show the change-detection accuracy patterns. It will be seen that PCCD decreased with increasing misregistration, and the value of PCCD was 0.9 when the value of RMSE was 0.6. Conversely, PMA, PFA, and PTE increased with increasing misregistration.

The image edges were then extracted using the Canny algorithm, and buffer zones were created at buffer distance values from 1 to 3 pixels based on the final edges, combining the t_1 and t_2 image edges. In the buffer zone with distance value 1, the change-detection errors are shown in Figure 9 for RMSE values from 0 to 1 pixels, and the commission, omission, and total error percentages falling within the buffer zone are illustrated for buffer distance values of 1, 2, and 3 in Figure 10.

As can be seen, when there was no image misregistration between two images, there were no commission errors, as shown in Figures 4 and 9(*a*), and PCEB was empty (Figure 10(*a*)). The value of both POEB and PTEB was 10% in this condition. For RMSE values from 0.2 to 0.6 pixels, the commission errors caused by misregistration almost all fell within the buffer zone, and POEB and PTEB increased and were close to 50% and 55%, respectively, at the RMSE value of 0.6 pixels (Figure 9(*a*)). When the RMSE value changed from 0.6 to 1 pixels, the commission errors always fell within the buffer zone, and the values of POEB and PTEB remained close to 50% and 55%, respectively, as shown in Figures 9(*f*) and 10(*a*). Two areas of Figure 9(*e*) are enlarged in Figures 9(*g*) and (h), indicating the detailed spatial distribution of commission and omission errors.

When the value of the buffer distance was 2, the commission errors almost all fell within the buffer zone, and both POEB and PTEB started at 20% when there was no misregistration and increased with increasing misregistration up to an RMSE value of 0.6 pixels, reaching 60% and 66%, respectively. They then remained stable, reaching nearly 62% and 70%, respectively, as shown in Figure 10(*b*). Furthermore, for distance value 3, the patterns of PCEB, POEB, and PTEB conform to those when the distance value was 2 pixels (Figure 10(*c*)). The commission errors almost all fell within the buffer zone. In contrast, both POEB and PTEB started from 30% when there was no misregistration, increased to 65% and 70%, respectively, with increasing misregistration up to the 0.6-pixel level, and remained stable and close to 70% and 75%, respectively, up to misregistration values of 1 pixel.

4. Discussion

Through experimentation, it was found that the registration accuracy required to achieve change-detection results of 90% accuracy is close to 0.6 pixels when only the misregistration factor is considered. Moreover, this conclusion is universal for medium- and high-resolution images (i.e. Landsat TM, ETM+, and Quickbird). It is worth noting that no matter which sensor acquired the images, the commission errors caused by misregistration

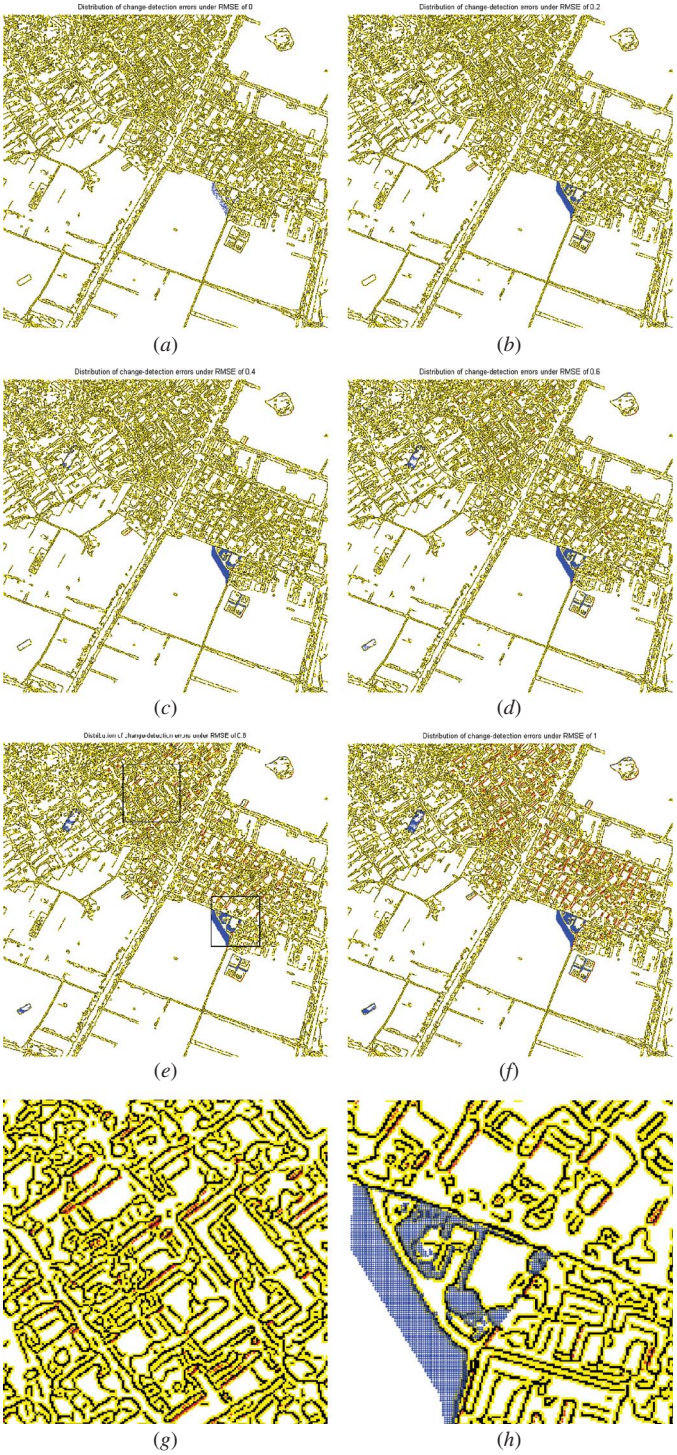

Figure 9. Spatial distribution of change-detection errors caused by misregistration based on the buffer zone for RMSE values from 0 to 1 pixels in steps of 0.2 pixels, corresponding to (*a*) to (*e*); (*g*) and (*h*) are enlarged views of upper and lower boxes in (*e*).

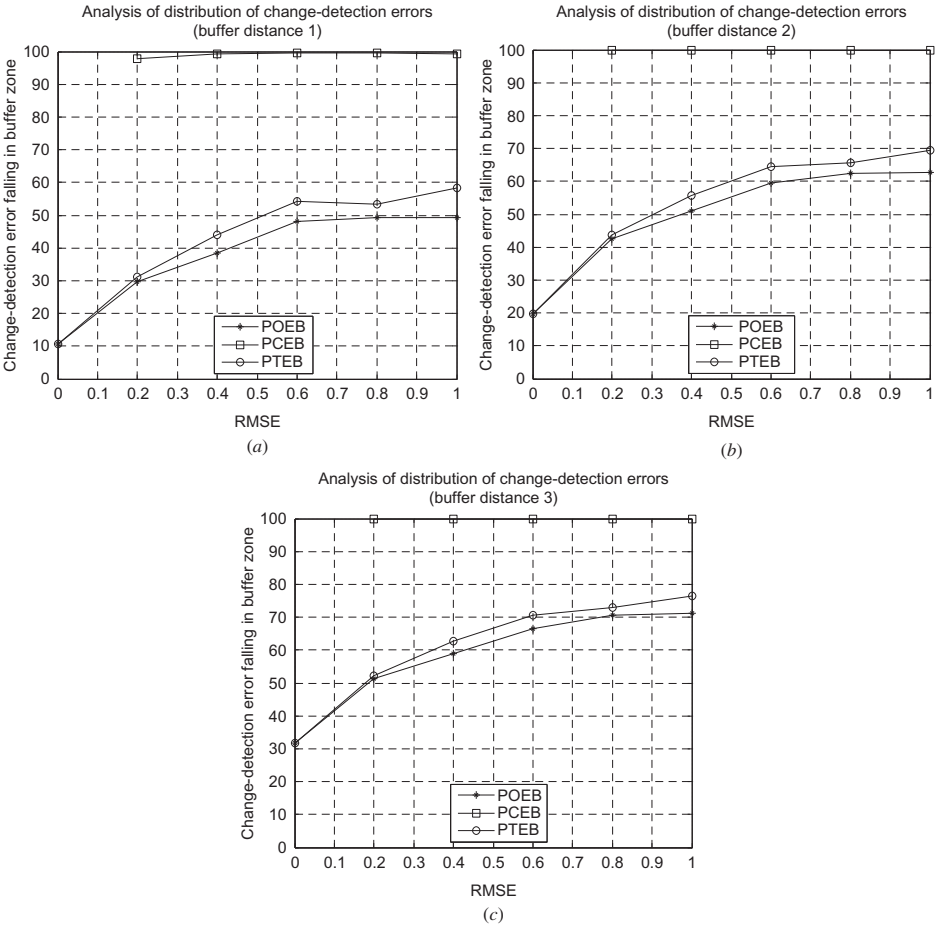

Figure 10. Percentage of change-detection errors including commission, omission, and total errors for different misregistrations falling within the buffer zone, with different distance values from 1 to 3 pixels corresponding to (*a*) to (*c*).

between 0 and 1 pixels almost all fall within the buffer zone for a distance value of 1 pixel created based on image edges. This means that commission errors occur mostly within 1 pixel of image edges.

For Landsat TM and ETM+ images, the omission errors caused by misregistration falling within the buffer zone reached 70% and 75%, respectively, and the percentage of total errors falling within the buffer zone was close to 80%. There is no need to set a buffer distance different from 1 for medium-resolution images. For Quickbird images, when the distance value of the buffer zone was 1, the percentage of commission errors falling within the buffer zone increased from 10% to 50% with increasing misregistration from 0 to 0.6 pixels, and then remained stable until an RMSE value of 1 pixel was reached. When the buffer distance value was 2 or 3 pixels, the spatial distribution pattern of commission and omission errors was similar to that when the distance value was 1 pixel, whereas the values of POEB and PTEB increased by about 10% for each increase in misregistration. In total, for medium-resolution images, about 70% of the omission errors fell within 1 pixel of the vicinity of multitemporal image edges. For high-resolution images, 50–60% of the omission errors fell within 1 or 2 pixels of image edges.

The edges account for 13.68%, 12.67%, and 10.18% in the images. For these different values, the commission errors have the same spatial distribution that almost all fall within 1 pixel of edges. In contrast, the omission errors have different spatial distribution for these different percentages of edges in the images. When the images have 13.68% and 12.67% edges, the spatial distributions of the omission errors are the same, where about 70% fall within 1 pixel of the edges. Only 50–60% of the omission errors fall within 1 or 2 pixels of the image edges when the image has 10.18% edges. Therefore, the spatial distribution of omission errors may be affected by the percentage of edges in the images. In short, this work shows, to a degree, the relations between change-detection errors due to misregistration and the edges of images. The outcomes indicate that edge and spatial information can be used to reduce the adverse effects of misregistration on change-detection accuracy.

5. Conclusions

The spatial distribution pattern of change-detection errors caused by misregistration was quantitatively analysed using buffering analysis based on combined multitemporal image edges. It was found that commission errors caused by misregistration occur mostly within 1 pixel of the image edges. In addition, 70% of omission errors appear within 1 pixel of the image edges for medium-resolution images and 50–60% of the omission errors occur within 1 or 2 pixels of the image edges for high-resolution images. A better understanding of this distribution would be very useful for developing new methods, which can potentially reduce the adverse effects of misregistration and increase change-detection accuracy. In addition, the spatial distribution of change-detection errors due to misregistration, conducted by the object-based method, merits further research due to the different nature of error distribution in comparison with pixel-based change detection.

Acknowledgements

The work presented in this article was supported by the Ministry of Science and Technology of China (Project No.: 2012BAJ15B04). The authors would like to thank the editor and the three anonymous reviewers whose insightful suggestions have significantly improved this article.

References

Bazi, Y., F. Melgani, and H. D. Al-Sharari. 2010. “Unsupervised Change Detection in Multispectral Remotely Sensed Imagery with Level Set Methods.” *IEEE Transactions on Geoscience and Remote Sensing* 48: 3178–3187.

Brown, K., G. Foody, and P. Atkinson. 2007. “Modelling Geometric and Misregistration Error in Airborne Sensor Data to Enhance Change Detection.” *International Journal of Remote Sensing* 28: 2857–2879.

Bruzzone, L., and R. Cossu. 2003. “An Adaptive Approach to Reducing Registration Noise Effects in Unsupervised Change Detection.” *IEEE Transactions on Geoscience and Remote Sensing* 41: 2455–2465.

Bruzzone, L., and D. F. Prieto. 2000. “Automatic Analysis of the Difference Image for Unsupervised Change Detection.” *IEEE Transactions on Geoscience and Remote Sensing* 38: 1171–1182.

Bruzzone, L., and S. Serpico. 1997. “Detection of Changes in Remotely-Sensed Images by the Selective Use of Multi-Spectral Information.” *International Journal of Remote Sensing* 18: 3883–3888.

Canny, J. 1986. “A Computational Approach to Edge Detection.” *IEEE Transactions on Pattern Analysis and Machine Intelligence* 8: 679–698.

Dai, X., and S. Khorram. 1998. “The Effects of Image Misregistration on the Accuracy of Remotely Sensed Change Detection.” *IEEE Transactions on Geoscience and Remote Sensing* 36: 1566–1577.

Ding, M., Z. Tian, Z. Jin, M. Xu, and C. Cao. 2010. "Registration Using Robust Kernel Principal Component for Object-Based Change Detection." *IEEE Geoscience and Remote Sensing Letters* 7: 761–765.

Lu, D., P. Mausel, E. Brondízio, and E. Moran. 2004. "Change Detection Techniques." *International Journal of Remote Sensing* 25: 2365–2401.

Marchesi, S., F. Bovolo, and L. Bruzzone. 2010. "A Context-Sensitive Technique Robust to Registration Noise for Change Detection in VHR Multispectral Images." *IEEE Transactions on Image Processing* 19: 1877–1889.

Melgani, F., and Y. Bazi. 2006. "Markovian Fusion Approach to Robust Unsupervised Change Detection in Remotely Sensed Imagery." *IEEE Geoscience and Remote Sensing Letters* 3: 457–461.

Singh, A. 1989. "Digital Change Detection Techniques Using Remotely-Sensed Data." *International Journal of Remote Sensing* 10: 989–1003.

Stow, D. 1999. "Reducing the Effects of Misregistration on Pixel-Level Change Detection." *International Journal of Remote Sensing* 20: 2477–2483.

Stow, D., L. Coulter, and S. Baer. 2003. "A Frame Centre Matching Approach to Registration for Change Detection with Fine Spatial Resolution Multi-Temporal Imagery." *International Journal of Remote Sensing* 24: 3873–3879.

Stow, D. A., and D. M. Chen. 2002. "Sensitivity of Multitemporal NOAA AVHRR Data of an Urbanizing Region to Land-Use/Land-Cover Changes and Misregistration." *Remote Sensing of Environment* 80: 297–307.

Sundaresan, A., P. K. Varshney, and M. K. Arora. 2007. "Robustness of Change Detection Algorithms in the Presence of Registration Errors." *Photogrammetric Engineering and Remote Sensing* 73: 375.

Townshend, J. R. G., C. O. Justice, C. Gurney, and J. McManus. 1992. "The Impact of Misregistration on Change Detection." *IEEE Transactions on Geoscience and Remote Sensing* 30: 1054–1060.

Zitova, B., and J. Flusser. 2003. "Image Registration Methods: A Survey." *Image and Vision Computing* 21: 977–1000.